JOC Featured Article

pubs.acs.org/joc

Construction of Peptoids with All *Trans*-Amide Backbones and Peptoid Reverse Turns via the Tactical Incorporation of *N*-Aryl Side Chains Capable of Hydrogen Bonding

Joseph R. Stringer, J. Aaron Crapster, Ilia A. Guzei, and Helen E. Blackwell*

Department of Chemistry, University of Wisconsin−Madison, 1101 University Avenue, Madison, Wisconsin 53706-1322

blackwell@chem.wisc.edu

Received June 3, 2010

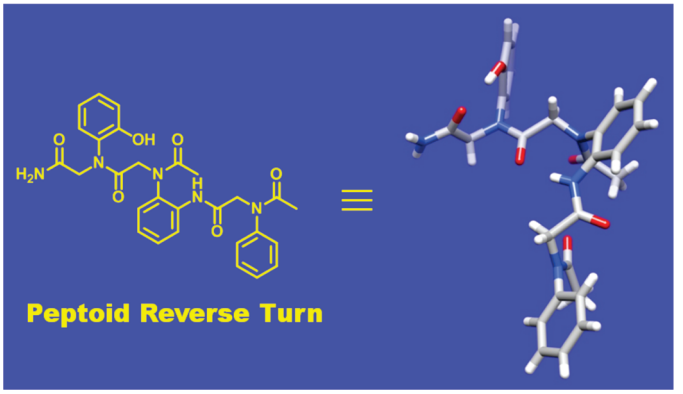

The ability to design foldamers that mimic the defined structural motifs of natural biopolymers is critical for the continued development of functional biomimetic molecules. Peptoids, or oligomers of *N*-substituted glycine, represent a versatile class of foldamers capable of folding into defined secondary and tertiary structures. However, the rational design of discretely folded polypeptoids remains a challenging task, due in part to an incomplete understanding of the covalent and noncovalent interactions that direct local peptoid folding. We have found that simple, peptoid monomer model systems allow for the effective isolation of individual interactions within the peptoid backbone and side chains and can facilitate the study of the role of these interactions in restricting local peptoid conformation. Herein, we present an analysis of a set of peptoid monomers and an oligomer containing *N*-aryl side chains capable of hydrogen bonding with the peptoid backbone. These model peptoids were found to exhibit well-defined local conformational preferences, allowing for control of the ω, ϕ, and ψ dihedral angles adopted by the systems. Fundamental studies of the peptoid monomers enabled the design and synthesis of an acyclic peptoid reverse-turn structure, in which *N*-aryl side chains outfitted with *ortho*-hydrogen bond donors were hypothesized to play a critical role in the stabilization of the turn. This trimeric peptoid was characterized by X-ray crystallography and 2D NMR spectroscopy and was shown to adopt a unique acyclic peptoid reverse-turn conformation. Further analysis of this turn revealed an $n\rightarrow\pi^*_{C=O}$ interaction within the peptoid backbone, which represents the first reported example of this type of stereoelectronic interaction occurring exclusively within a polypeptoid backbone. The installation of *N*-aryl side chains capable of hydrogen bonding into peptoids is straightforward and entirely compatible with current solid-phase peptoid synthesis methodologies. As such, we anticipate that the strategic incorporation of these *N*-aryl side chains should facilitate the construction of peptoids capable of adopting discrete structural motifs, both turnlike and beyond, and will facilitate the continued development of well-folded peptoids.

 Published on Web 08/19/2010 DOI: 10.1021/jo101075a

Introduction

Biomimicry by non-natural polymers remains a challenging task. However, extensive efforts toward the development of foldameric systems that mimic the structure and function of Nature's biopolymers have provided significant insight into the folding propensities and functions of a variety of abiotic polymers.[1] Peptoids, or oligomers of *N*-substituted glycine, have emerged as an important class of peptidomimetic foldamer, in part because they have shown the ability to perform a range of relevant and specific biological functions, including inhibiting certain protein−protein interactions,[2,3] acting as potent and selective antimicrobial agents,[4,5] and serving as molecular transporters.[6,7] Additionally, peptoids offer attractive advantages relative to native α-peptide scaffolds due to their increased cellular permeability,[8,9] proteolytic stability,[10] straightforward and modular synthesis,[11] and ability to display a wide range of non-native functionalities.[12−14] For the continued development of peptoids as functional mimics of biological macromolecules, however, there remains a need to generate peptoid oligomers capable of folding into predictable and distinct three-dimensional structures. Although it has been demonstrated that well-defined structure is not essential for peptoid function in certain specific cases,[2] the ability to accurately construct peptoids with a variety of well-defined secondary (and higher order) structures could open up new avenues for their use in biological applications.

Thus far, the best-characterized peptoid secondary structure is the peptoid helix, which resembles a polyproline type I helix with approximately three residues per turn and a helical pitch of approximately 6.7 Å per turn.[15−17] These structures are limited to a relatively small set of peptoid primary sequences, largely based on residues containing sterically bulky, α-chiral side chains. Such sterically demanding side chains have been found to enforce largely *cis*-amide bond geometries in peptoid backbone amides, thereby reducing overall peptoid conformational flexibility. Recently, Kirshenbaum and co-workers have reported complementary efforts toward the design of peptoid helices that mimic the polyproline type II helix.[18] These strategies have focused on using achiral, *N*-aryl side chains, which force the peptoid backbone amides to adopt predominately *trans*-amide conformations, primarily due to steric[19,20] and electronic factors.[18,20] In the Kirshenbaum work, molecular modeling predicted that an *N*-aryl peptoid hexamer could form extended right- and left-handed polyproline type II helices, with approximately 3.1 residues per turn and a helical pitch of approximately 9 Å per turn. Experimental studies of these helices are ongoing and are of significant interest as *trans*-amide polypeptoids may adopt structures beyond the polyproline type II helix, such as peptoid sheetlike structures.

In addition to peptoid helices, several recent investigations have focused on the design and characterization of peptoid loops and turns. The peptoid "threaded" loop represents a secondary structure unique to peptoids and was first characterized by Huang et al.[21] This lasso-like motif appears to be limited to a very small set of peptoid primary sequence space, that is, peptoid nonamers of bulky α-chiral peptoid residues. The loop is formed by the peptoid backbone doubling back on itself via the formation of intramolecular hydrogen bonds between the *N*-terminal amine and several backbone amides and has been well characterized in solution by NMR spectroscopy. In contrast to loops, turn motifs are common secondary structural elements in polypeptides,[22−24] and the development of peptoid turns is justifiably of significant interest. Notable examples by Appella,[25] Kirshenbaum,[26] and co-workers highlight recent advancements in peptoid turn design, including both cyclic peptoid turns and acyclic peptide−peptoid hybrids. These initial studies demonstrate that peptoids can fold into well-defined turn motifs that can mimic naturally occurring turns in polypeptides.[26] However, further work is required to develop a standard set of design strategies for the formation of acyclic peptoid turns in the context of polypeptoid structures.

Despite the examples outlined above, the number of reported peptoid secondary structures and studies thereof remains relatively small in comparison to other foldameric systems.[27,28] This is largely due to the poor understanding of

(1) Gellman, S. H. *Acc. Chem. Res.* **1998**, *31*, 173–180.
(2) Hara, T.; Durell, S. R.; Myers, M. C.; Appella, D. H. *J. Am. Chem. Soc.* **2006**, *128*, 1995–2004.
(3) Udugamasooriya, D. G.; Dineen, S. P.; Brekken, R. A.; Kodadek, T. *J. Am. Chem. Soc.* **2008**, *130*, 5744–5752.
(4) Chongsiriwatana, N. P.; Patch, J. A.; Czyzewski, A. M.; Dohm, M. T.; Ivankin, A.; Gidalevitz, D.; Zuckermann, R. N.; Barron, A. E. *Proc. Natl. Acad. Sci. U.S.A.* **2008**, *105*, 2794–2799.
(5) Patch, J. A.; Barron, A. E. *J. Am. Chem. Soc.* **2003**, *125*, 12092–12093.
(6) Murphy, J. E.; Uno, T.; Hamer, J. D.; Cohen, F. E.; Dwarki, V.; Zuckermann, R. N. *Proc. Natl. Acad. Sci. U.S.A.* **1998**, *95*, 1517–1522.
(7) Wender, P. A.; Mitchell, D. J.; Pattabiraman, K.; Pelkey, E. T.; Steinman, L.; Rothbard, J. B. *Proc. Natl. Acad. Sci. U.S.A.* **2000**, *97*, 13003–13008.
(8) Kwon, Y.-U.; Kodadek, T. *J. Am. Chem. Soc.* **2007**, *129*, 1508–1509.
(9) Tan, N. C.; Yu, P.; Kwon, Y.-U.; Kodadek, T. *Bioorg. Med. Chem.* **2008**, *16*, 5853–5861.
(10) Miller, S. M.; Simon, R. J.; Ng, S.; Zuckermann, R. N.; Kerr, J. M.; Moos, W. H. *Bioorg. Med. Chem. Lett.* **1994**, *4*, 2657–2662.
(11) Zuckermann, R. N.; Kerr, J. M.; Kent, S. B. H.; Moos, W. H. *J. Am. Chem. Soc.* **1992**, *114*, 10646–10647.
(12) Burkoth, T. S.; Fafarman, A. T.; Charych, D. H.; Connolly, M. D.; Zuckermann, R. N. *J. Am. Chem. Soc.* **2003**, *125*, 8841–8845.
(13) Horn, T.; Lee, B.-C.; Dill, K. A.; Zuckermann, R. N. *Bioconjugate Chem.* **2004**, *15*, 428–435.
(14) Uno, T.; Beausoleil, E.; Goldsmith, R. A.; Levine, B. H.; Zuckermann, R. N. *Tetrahedron Lett.* **1999**, *40*, 1475–1478.
(15) Armand, P.; Kirshenbaum, K.; Goldsmith, R. A.; Farr-Jones, S.; Barron, A. E.; Truong, K. T. V.; Dill, K. A.; Mierke, D. F.; Cohen, F. E.; Zuckermann, R. N.; Bradley, E. K. *Proc. Natl. Acad. Sci. U.S.A.* **1998**, *95*, 4309–4314.
(16) Kirshenbaum, K.; Barron, A. E.; Goldsmith, R. A.; Armand, P.; Bradley, E. K.; Truong, K. T. V.; Dill, K. A.; Cohen, F. E.; Zuckermann, R. N. *Proc. Natl. Acad. Sci. U.S.A.* **1998**, *95*, 4303–4308.
(17) Wu, C. W.; Kirshenbaum, K.; Sanborn, T. J.; Patch, J. A.; Huang, K.; Dill, K. A.; Zuckermann, R. N.; Barron, A. E. *J. Am. Chem. Soc.* **2003**, *125*, 13525–13530.
(18) Shah, N. H.; Butterfoss, G. L.; Nguyen, K.; Yoo, B.; Bonneau, R.; Rabenstein, D. L.; Kirshenbaum, K. *J. Am. Chem. Soc.* **2008**, *130*, 16622–16632.
(19) Itai, A.; Toriumi, Y.; Saito, S.; Kagechika, H.; Shudo, K. *J. Am. Chem. Soc.* **1992**, *114*, 10649–10650.
(20) Saito, S.; Toriumi, Y.; Tomioka, N.; Itai, A. *J. Org. Chem.* **1995**, *60*, 4715–4720.
(21) Huang, K.; Wu, C. W.; Sanborn, T. J.; Patch, J. A.; Kirshenbaum, K.; Zuckermann, R. N.; Barron, A. E.; Radhakrishnan, I. *J. Am. Chem. Soc.* **2006**, *128*, 1733–1738.
(22) Schneider, J. P.; Kelly, J. W. *Chem. Rev.* **1995**, *95*, 2169–2187.
(23) Robinson, J. A. *Acc. Chem. Res.* **2008**, *41*, 1278–1288.
(24) Burgess, K. *Acc. Chem. Res.* **2001**, *34*, 826–835.
(25) Pokorski, J. K.; Miller Jenkins, L. M.; Feng, H.; Durell, S. R.; Bai, Y.; Appella, D. H. *Org. Lett.* **2007**, *9*, 2381–2383.
(26) Shin, S. B. Y.; Yoo, B.; Todaro, L. J.; Kirshenbaum, K. *J. Am. Chem. Soc.* **2007**, *129*, 3218–3225.
(27) Goodman, C. M.; Choi, S.; Shandler, S.; DeGrado, W. F. *Nat. Chem. Biol.* **2007**, *3*, 252–262.
(28) Hill, D. J.; Mio, M. J.; Prince, R. B.; Hughes, T. S.; Moore, J. S. *Chem. Rev.* **2001**, *101*, 3893–4011.

peptoid folding processes in general. To date, steric,[15] hydrophobic,[21] electrostatic,[29] stereoelectronic,[30] and hydrogen-bonding interactions[21,31] have been implicated in local and global peptoid folding. Careful investigation of the specific noncovalent interactions that govern peptoid folding would undoubtedly aid in future peptoid design. Furthermore, previous work has focused primarily on controlling amide bond geometry (ω dihedral angle) in peptoids. However, in addition to the ω angle, the ϕ and ψ dihedral angles are also subject to change and thus contribute, in part, to the overall conformational flexibility of peptoids. For example, the recent modeling studies of Kirshenbaum and co-workers have suggested that, in addition to *cis*/*trans* ω amide bond isomerization, there exists considerable flexibility in ψ when a *trans* ω geometry is present.[32] Therefore, the installation of side chains that are capable of predictably influencing the rotational preferences of the ϕ and ψ dihedral angles, in addition to the ω dihedral angle, may serve as a general tactic for reducing overall conformational flexibility in polypeptoids. To address these challenges, our group is studying the mechanisms of peptoid folding by probing the effects of various side chain-to-backbone and backbone-to-backbone noncovalent interactions on ω, ϕ, and ψ dihedral angles in model peptoid systems.[30,31,33,34] We have focused our efforts on monomers that are straightforward to synthesize and install using established peptoid synthesis techniques, thereby enabling their facile incorporation into polypeptoids. Using this fundamental approach, we seek to contribute to a more complete understanding of peptoid sequence−structure relationships and facilitate the future rational design of peptoids with novel secondary and higher order structures.

Herein, we report the design, synthesis, and characterization of a series of peptoids equipped with *N*-aryl side chains capable of hydrogen bonding with the peptoid backbone. These studies demonstrate that the presence of such hydrogen-bonding side chains can strongly affect local backbone conformational preferences in peptoid monomers and oligomers—both in solution and in the solid state—and allow for greater control over the ω, ϕ, and ψ dihedral angles adopted by these systems relative to peptoids containing analogous *N*-aryl side chains that are incapable of hydrogen bonding. On the basis of these results, we rationally designed and synthesized an acyclic peptoid reverse turn and characterized its structure in solution by two-dimensional nuclear magnetic resonance (2D NMR) spectroscopy and in the solid state by single-crystal X-ray crystallography. Further analysis of this peptoid reverse-turn structure revealed an $n\rightarrow\pi^*_{C=O}$ interaction within the peptoid backbone, which represents the first reported example of this type of stereoelectronic interaction occurring exclusively within a polypeptoid backbone.[35] We anticipate that the design strategies presented herein incorporating *N*-aryl side chains should advance the understanding of peptoid folding and the ongoing development of a generalized set of peptoid folding rules.

Results and Discussion

Motivation. We sought to examine whether noncovalent interactions between substituted *N*-aryl peptoid side chains and the peptoid backbone could be utilized to engender predictable conformational motifs in peptoids. As highlighted above, recent investigations by Kirshenbaum and co-workers had shown that *N*-aryl side chains enforce predominantly *trans* backbone amides in peptoids.[18] We reasoned that substituents on the aryl ring could be utilized to enforce additional, unique restrictions on local peptoid conformation. Prior to designing such peptoids, further scrutiny of the unsubstituted *N*-aryl systems was required, and we sought to do so in the context of our previously reported, peptoid monomer model system.[30,34] We therefore analyzed *N*-aryl monomer peptoid **1** (Figure 1A) as a control compound. Previous studies in our laboratory have shown that monomeric peptoids, such as **1**, can be reliable model systems for the isolation and examination of noncovalent interactions in peptoids, while mimicking the local environment of typical polypeptoids.[30,34]

N-Aryl peptoid monomer **1** was synthesized according to our previously reported method[30] and characterized by NMR spectroscopy and X-ray crystallography (see the Experimental Section for details of NMR and X-ray analyses). The 1D-NOESY and ^{1}H NMR spectra for **1** revealed that the *N*-aryl amide bond displayed a $>95\%$ preference for the *trans*-amide in $CDCl_3$ at 25 °C (see the Supporting Information). In turn, the X-ray crystal structure of **1** (Figure 1B) revealed an *N*-terminal *trans*-amide bond and the *N*-aryl side chain rotated out of the plane ~66° relative to the peptoid backbone. These data support those reported by Kirshenbaum and co-workers and others for related peptoid[18] and amide model systems.[19,20,37,38] Careful inspection of the solid-state structure of **1** led us to speculate that *ortho*-substituted *N*-aryl side chains may engender subtle, but distinct, local rotational preferences among backbone dihedral angles relative to those of previously studied *N*-aryl peptoids. We hypothesized that the placement of a hydrogen-bond donor at the *ortho* position could have a dramatic effect, as it would offer a potential tunable strategy to effectively restrict rotation about local single bonds and thus confer additional conformational ordering to *N*-aryl peptoids. Specifically, based on our studies of **1** in the solid state, we reasoned that this functionality would be ideally suited to form an intramolecular 8-membered-ring hydrogen bond to the *C*-terminal carbonyl oxygen. However, we note that an alternate hydrogen bond is also possible between the *N*-aryl hydrogen bond donor and the *N*-terminal carbonyl oxygen, which would result in a 7-membered ring instead (see Figure 1C). We therefore set forth to design, synthesize, and characterize peptoid monomer model systems and peptoid oligomers

(29) Shin, S. B. Y.; Kirshenbaum, K. *Org. Lett.* **2007**, *9*, 5003–5006.
(30) Gorske, B. C.; Bastian, B. L.; Geske, G. D.; Blackwell, H. E. *J. Am. Chem. Soc.* **2007**, *129*, 8928–8929.
(31) Gorske, B. C.; Blackwell, H. E. *J. Am. Chem. Soc.* **2006**, *128*, 14378–14387.
(32) Butterfoss, G. L.; Renfrew, P. D.; Kuhlman, B.; Kirshenbaum, K.; Bonneau, R. *J. Am. Chem. Soc.* **2009**, *131*, 16798–16807.
(33) Fowler, S. A.; Luechapanichkul, R.; Blackwell, H. E. *J. Org. Chem.* **2009**, *74*, 1440–1449.
(34) Gorske, B. C.; Stringer, J. R.; Bastian, B. L.; Fowler, S. A.; Blackwell, H. E. *J. Am. Chem. Soc.* **2009**, *131*, 16555–16567.
(35) On the basis of molecular modeling studies, $n\rightarrow\pi^*_{C=O}$ interactions between adjacent *trans*-amide bonds have been suggested as possible stabilizing influences on a peptoid polyproline type II helix. See ref 18.
(36) Moehle, K.; Hofmann, H.-J. *Biopolymers* **1996**, *38*, 781–790.
(37) Itai, A.; Toriumi, Y.; Tomioka, N.; Kagechika, H.; Azumaya, I.; Shudo, K. *Tetrahedron Lett.* **1989**, *30*, 6177–6180.
(38) Pedersen, B. F.; Pedersen, B. *Tetrahedron Lett.* **1965**, 2995–3001.

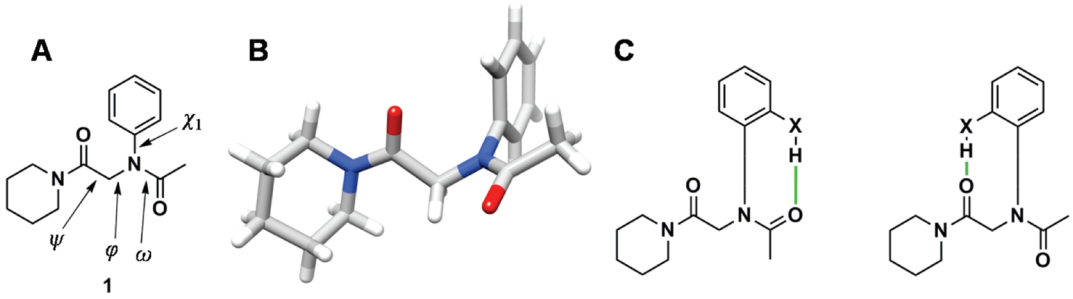

FIGURE 1. (A) Chemical structure of peptoid monomer model system **1** showing dihedral angles as previously described in peptoids.[32,36] (B) X-ray crystal structure of **1** showing the *trans*-amide geometry and the *N*-aryl side chain rotated out of the amide plane. (C) Chemical structure showing a hypothetical 7-membered-ring (left) and 8-membered-ring (right) hydrogen bond (solid green line) in a peptoid monomer containing an *o*-aryl hydrogen-bond donor.

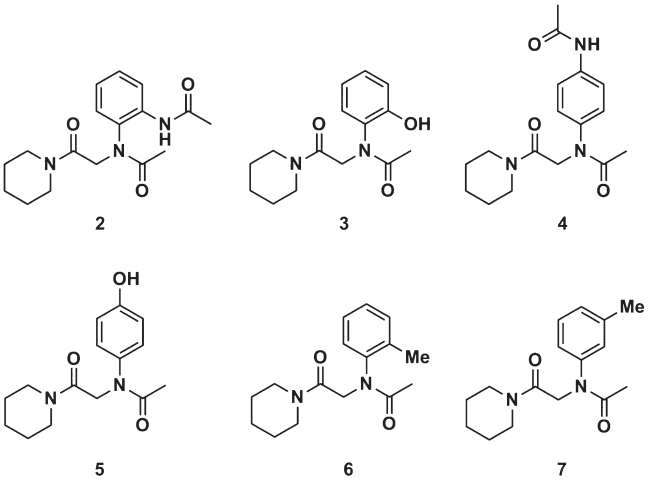

FIGURE 2. Chemical structures of peptoid monomer model systems **2**−**7**.

containing hydrogen-bonding *N*-aryl side chains to probe our hypotheses. The results and implications of these studies are reported below.

Design and Synthesis of *N*-Aryl Peptoid Monomers. We examined six *N*-aryl peptoid monomer model systems in this study (**2**−**7**; shown in Figure 2). Monomers **2** and **3** were designed to investigate potential interactions of *o*-acetamide and *o*-hydroxyl hydrogen-bond donors, respectively. Peptoid monomers **4** and **5** were generated as control compounds in order to characterize the nature of any potential hydrogen-bonding interactions observed in monomers **2** and **3**. The *para* positioning of the hydrogen-bonding substituents in both **4** and **5** precludes the formation of an intramolecular hydrogen bond but allows for the possibility of intermolecular hydrogen-bonding interactions.

For comparison to the hydrogen-bonding monomers **2**−**5**, we also sought to investigate the effects of non-hydrogen-bonding, *ortho*-substituted *N*-aryl side chains on peptoid local conformation. We therefore synthesized monomers **6** and **7**, which contain methyl-substituted *N*-aryl side chains that cannot participate in hydrogen bonding and differ only in the substitution pattern on their aryl ring, as controls. All six monomers were generated in high purity using our previously reported, straightforward synthetic route to diamide peptoid model systems.[30,34]

Characterization of Peptoid Monomers 2−7 in Solution. We first characterized the structures of peptoid monomers **2**−**7** in solution using NMR spectroscopy. In order to be applicable as a modular design strategy in polypeptoids, an ideal hydrogen-bonding interaction in the substituted *N*-aryl peptoids would involve both a unique hydrogen-bond donor and a unique acceptor. Again, an intramolecular hydrogen bond in monomers **2** and **3** could involve either the *C*-terminal carbonyl oxygen or the *N*-terminal carbonyl oxygen as a hydrogen-bond acceptor (see Figure 1C). In the latter case, the *N*-aryl amide bond must be in the *cis*-amide geometry for the resulting intramolecular 7-membered-ring hydrogen bond to occur. Such a geometry would be unexpected in light of the data above for peptoid **1** indicating it adopted a predominantly *trans*-amide geometry. NOESY experiments in $CDCl_3$ at room temperature confirmed the *N*-aryl amide bond in **2** displayed a 93% preference for the *trans*-amide, while **3** displayed a >95% preference for the *trans*-amide. These NMR data suggest that since the *N*-aryl amide bonds in **2** and **3** exist almost entirely as *trans*-amides, conformational states containing an intramolecular 7-membered-ring hydrogen bond to the *N*-terminal carbonyl oxygen are not significantly populated in **2** or **3** under these conditions.

To further examine the nature of potential hydrogen-bonding interactions in peptoid monomers **2** and **3**, we utilized variable-concentration ^{1}H NMR studies. Such ^{1}H NMR studies can provide insight into the presence of inter- vs intramolecular hydrogen-bonding interactions in solution and are frequently utilized for this purpose in foldamer research.[39−42] Protons involved in intermolecular hydrogen bonding most commonly display concentration-dependent chemical shift values, while protons involved in intramolecular hydrogen bonding exhibit chemical shifts that are concentration independent.[43] Variable concentration ^{1}H NMR studies of monomers **2** and **3**, along with control monomers **4** and **5**, were carried out at 0.1−100 mM in $CDCl_3$ at room temperature (Figure 3). Over this concentration range, $\Delta\delta$ (**2**)-NH = 0.0 and $\Delta\delta$ (**3**)-OH = 0.0, consistent with intramolecular hydrogen bonding. In contrast, $\Delta\delta$ (**4**)-NH = 3.2 and $\Delta\delta$ (**5**)-OH = 1.3 over the same concentration range, consistent with intermolecular hydrogen bonding. Additionally, the significant

(39) Dado, G. P.; Gellman, S. H. *J. Am. Chem. Soc.* **1993**, *115*, 4228–4245.
(40) Prabhakaran, P.; Kale, S. S.; Puranik, V. G.; Rajamohanan, P. R.; Chetina, O.; Howard, J. A. K.; Hofmann, H.-J.; Sanjayan, G. J. *J. Am. Chem. Soc.* **2008**, *130*, 17743–17754.
(41) Eyman, D. P.; Drago, R. S. *J. Am. Chem. Soc.* **1966**, *88*, 1617–1620.
(42) Gellman, S. H.; Dado, G. P.; Liang, G. B.; Adams, B. R. *J. Am. Chem. Soc.* **1991**, *113*, 1164–1173.
(43) Haque, T. S.; Little, J. C.; Gellman, S. H. *J. Am. Chem. Soc.* **1994**, *116*, 4105–4106.

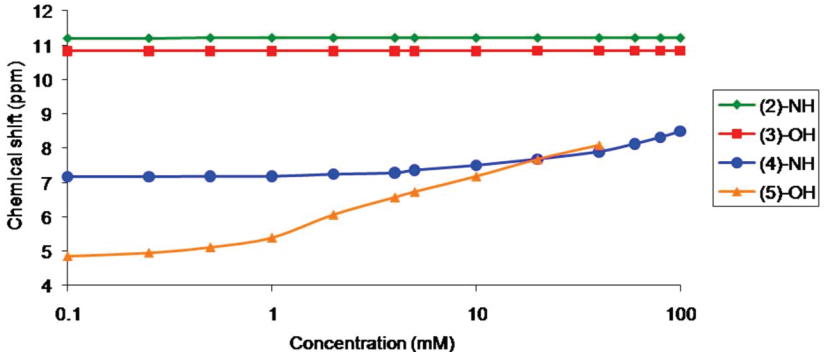

FIGURE 3. NMR chemical shifts of the hydrogen-bond donor protons in peptoids **2**−**5** plotted as a function of the logarithm of peptoid concentration (in $CDCl_3$, 25 °C). Data for peptoid **5** at concentrations ≥60 mM are not reported due to its lowered solubility at these concentrations.

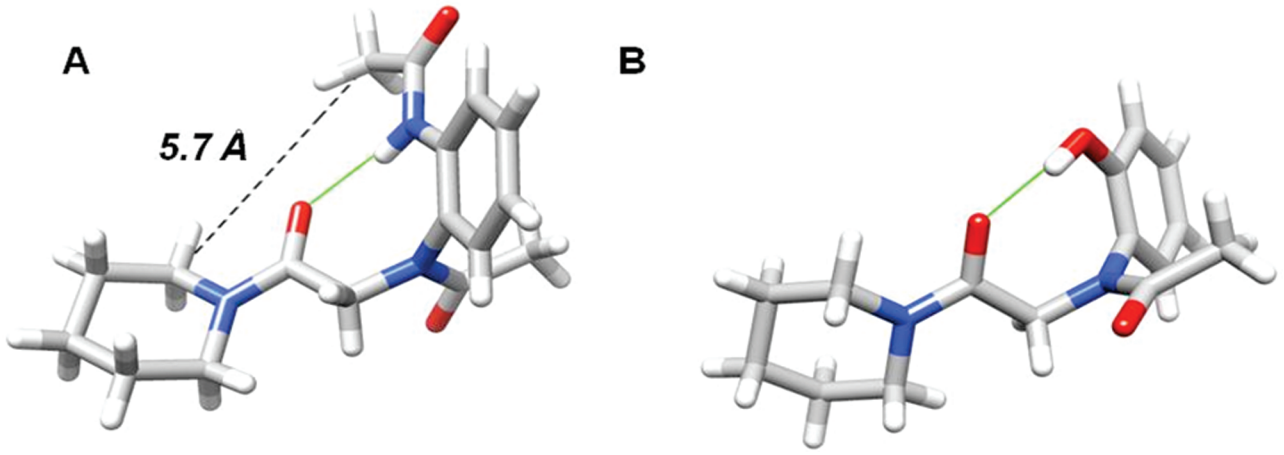

FIGURE 4. X-ray crystal structures of peptoid monomers (A) **2** and (B) **3**. Hydrogen bonds (solid green lines) and interatomic distance (black dashed line) are shown. Hydrogen bond in **2**: N···O distance = 2.79 Å. Hydrogen bond in **3**: O···O distance = 2.66 Å.

downfield chemical shifts of (**2**)-NH and (**3**)-OH, relative to the upfield shifts of (**4**)-NH and (**5**)-OH, are consistent with intramolecular hydrogen-bonding interactions. These NMR data support our initial hypothesis that an intramolecular 8-membered-ring hydrogen bond is present in peptoid monomers **2** and **3** and that intermolecular hydrogen-bonding interactions exist, at least to some degree, in control monomers **4** and **5**.

Our NMR analysis also revealed that the methylene protons in the *ortho*-substituted *N*-aryl peptoid monomers **2**, **3**, **6**, and **7** are all diastereotopic (see the Supporting Information for spectra). These observations are in agreement with previously reported studies by Siddall et al. on *ortho*-substituted acetanilides structurally similar to **6** and **7**.[44−47] This phenomenon is a result of atropisomerism due to restricted rotation of the *ortho*-substituted *N*-aryl moiety around the nitrogen−aryl bond. Our NMR data suggest that *ortho*-substitution of the *N*-aryl side chain, as in monomers **2**, **3**, **6**, and **7**, results in atropisomerism, regardless of the hydrogen-bonding capability of the side chain. Therefore, it may be possible to use *ortho*-substituted *N*-aryl side chains that do not contain a hydrogen-bond donor, such as those in **6** and **7**, to restrict side chain rotation and potentially influence local torsions within the peptoid backbone. Unfortunately, our inability to characterize monomers **6** or **7** by X-ray crystallography hindered further structural comparisons to the hydrogen-bond-containing monomers **2** and **3**.

Characterization of Peptoid Monomers 2 and 3 in the Solid State. To provide additional supporting evidence that the *N*-aryl side chains in peptoid monomers **2** and **3** influence local peptoid conformations, we analyzed their solid-state conformations by single-crystal X-ray crystallography. Crystals of **2** and **3** were grown by slow evaporation from a CH_2Cl_2/*n*-hexane solution at room temperature (see the Experimental Section). Notably, monomers **2** and **3** each crystallized as single enantiomers throughout their respective crystal lattices. The X-ray crystal structure of peptoid monomer **2** revealed an intramolecular 8-membered-ring hydrogen bond between the side chain amide proton and *C*-terminal carbonyl oxygen (Figure 4A). Similarly, the X-ray crystal structure of **3** showed an intramolecular 8-membered-ring hydrogen bond between the side chain hydroxyl proton and *C*-terminal carbonyl oxygen (Figure 4B). In both monomers, the *C*-terminal carbonyl oxygen acts as the sole hydrogen-bond acceptor in the intramolecular hydrogen bond. Further, the hydrogen bonds in **2** and **3** are exclusively intramolecular in their

(44) Siddall, T. H.; Prohaska, C. A. *Nature* **1965**, *208*, 582–583.
(45) Siddall, T. H., III; Prohaska, C. A. *J. Am. Chem. Soc.* **1966**, *88*, 1172–1176.
(46) Siddall, T. H., III; Stewart, W. E. *J. Org. Chem.* **1969**, *34*, 2927–2933.
(47) Siddall, T. H., III; Stewart, W. E. *J. Phys. Chem.* **1969**, *73*, 40–45.

TABLE 1. Dihedral Angles Observed in X-ray Crystal Structures of Peptoid Monomers 1−3

peptoid	ϕ (deg)	ψ (deg)	χ_1 (deg)	ω (deg)
1	101.00	167.79	114.71	179.05
2	−79.21	162.45	82.92	−179.31
3	74.55	−165.27	106.33	−179.36

respective crystal lattices, again with the *C*-terminal carbonyl oxygens acting as the lone hydrogen-bond acceptors. These solid-state data for peptoid monomers **2** and **3** corroborate the corresponding NMR data discussed above and suggest that the conformational state containing an intramolecular 8-membered-ring hydrogen bond is highly populated by these two peptoid monomers, both in solution and in the solid state.

The dihedral angles observed in the X-ray crystal structures of peptoid monomers **1**−**3** are listed in Table 1 (see Figure 1 for angle designations in peptoids). We note that since either enantiomer of **1**−**3** could potentially exist in solution or in the solid state, only absolute values need be considered when comparing the dihedral angles in Table 1. All three peptoid monomers have *trans*-amide bonds[17,18,48] (ω) with values (∼179° each) near planarity. The ψ values in **1**−**3** are also similar, ranging from 162.45° to 167.79°, but the ϕ values in *ortho*-substituted monomers **2** (−79.21°) and **3** (74.55°) differ from the unsubstituted aryl peptoid monomer **1** (101.00°). This difference in ϕ values in **2** and **3** relative to **1** may be a result of the intramolecular hydrogen bond, which stabilizes the backbone orientations in **2** and **3**. Further comparisons to other previously reported *N*-aryl peptoid structures are complicated, as these *N*-aryl structures are either part of a peptoid macrocycle or contain intermolecular hydrogen bonding.[18] We therefore chose to directly compare the values in Table 1 to a peptoid oligomer (**9**, see below) containing side chains derived from monomers **1**−**3**, and we return to this comparison below.

Further inspection of the X-ray crystal structure of *o*-acetamide monomer **2** indicated that the distance between the *N*-terminal methyl carbon and *C*-terminal piperidinyl carbon α to the nitrogen is 5.7 Å (Figure 4A). Interestingly, this distance is within the distance constraints of typical peptide turns (Cα···Cα distance ≤ 7 Å).[49,50] We therefore envisaged that the *o*-acetamide *N*-aryl side chain in **2** could be used as a novel reverse-turn-forming motif in peptoid oligomers, in which the turn backbone would continue from the *o*-acetamide nitrogen as opposed to the adjacent, "native" *N*-terminus. Such an acyclic turn structure had yet to be evaluated in peptoids and could be straightforward to implement. We outline our application of this new design strategy below.

Design and Synthesis of a Peptoid Reverse Turn. We designed an acyclic, trimeric peptoid turn (**9**) containing the *o*-amide *N*-aryl side chain from peptoid monomer **2** as a turn-inducing motif (Figure 5). We then flanked this central unit (residue 2) with two *N*-aryl peptoid residues that would enforce *trans*-amide geometries in the peptoid backbone. These flanking *trans*-amide residues were anticipated

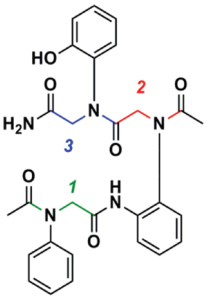

FIGURE 5. Chemical structure of peptoid **9** with individual residues color-coded: green, derived from monomer **1**; red, derived from monomer **2**; blue, derived from monomer **3**.

to position the termini backbone atoms directly opposite each other in an approximate antiparallel orientation. Accordingly, we selected the unsubstituted and *o*-hydroxyl *N*-aryl residues (derived from peptoid monomers **1** and **3**) for the *N*- and *C*-termini (residues 1 and 3), respectively. Again, the central *o*-amide *N*-aryl side chain would constitute part of the actual turn backbone, with the third *N*-aryl residue coupled to the *o*-amide substituent. Notably, this turn design would allow us to study not only the ability of the *o*-acetamide *N*-aryl unit to induce a turn in peptoids but also the effects of the three *N*-aryl side chains of monomers **1**−**3** on peptoid backbone amide geometries in an actual oligomeric peptoid system (vide infra).

We developed a solid-phase synthetic route to peptoid turn **9** on a Rink amide linker-derivatized resin that built on our previously reported, microwave-assisted peptoid synthesis procedure (Scheme 1).[11,51] This route uses the two-step submonomer method to generate each peptoid unit via a bromoacetic acid coupling and a subsequent nucleophilic displacement with a primary amine.[11] Peptoid trimer **9** was thus constructed using three iterative acid and amine couplings. Due to the low nucleophilicity of aryl amines, bromoacetylation and amination reactions required extended reaction times relative to those typical for *N*-alkyl peptoid syntheses (1.5 and 16 h at rt vs ∼20 min and ∼20 min at rt, respectively).[11] We found that performing the amination reactions at 60 °C using microwave irradiation for 1 h expedited the installation of the two flanking *N*-aryl side chains in **9**.[18,51] The central turn-inducing motif was installed using *N*-Fmoc-protected 2-amino aniline **8**, which was readily synthesized in solution on gram scale. We chose to perform this amination at room temperature for 16 h to reduce potential thermal cleavage of the *N*-Fmoc group. Acetylation of the central turn inducing motif, and ultimately the *N*-terminus, was achieved via bromoacetylation and subsequent reduction using $NaBH_4$.[51] Crude peptoid **9** was isolated by acid-mediated resin cleavage (using TFA), purified by flash silica gel chromatography, and characterized by MS to confirm its identity (see the Experimental Section). Using these methods, pure **9** could be generated on a ∼20 mg scale.

Characterization of Peptoid 9 in Solution. We evaluated the solution-phase conformation of peptoid **9** in $CDCl_3$ at 10 mM using NMR spectroscopy. 1D ^{1}H NMR data suggested that **9** exists as a mixture of one major conformer family (∼70% populated based on integration) and several minor

(48) Sui, Q.; Borchardt, D.; Rabenstein, D. L. *J. Am. Chem. Soc.* **2007**, *129*, 12042–12048.
(49) Lewis, P. N.; Momany, F. A.; Scheraga, H. A. *Biochim. Biophys. Acta, Protein Struct.* **1973**, *303*, 211–229.
(50) Ball, J. B.; Hughes, R. A.; Alewood, P. F.; Andrews, P. R. *Tetrahedron* **1993**, *49*, 3467–3478.
(51) Shah, N. H.; Kirshenbaum, K. *Org. Biomol. Chem.* **2008**, *6*, 2516–2521.

SCHEME 1. Synthesis of Peptoid Trimer 9[a]

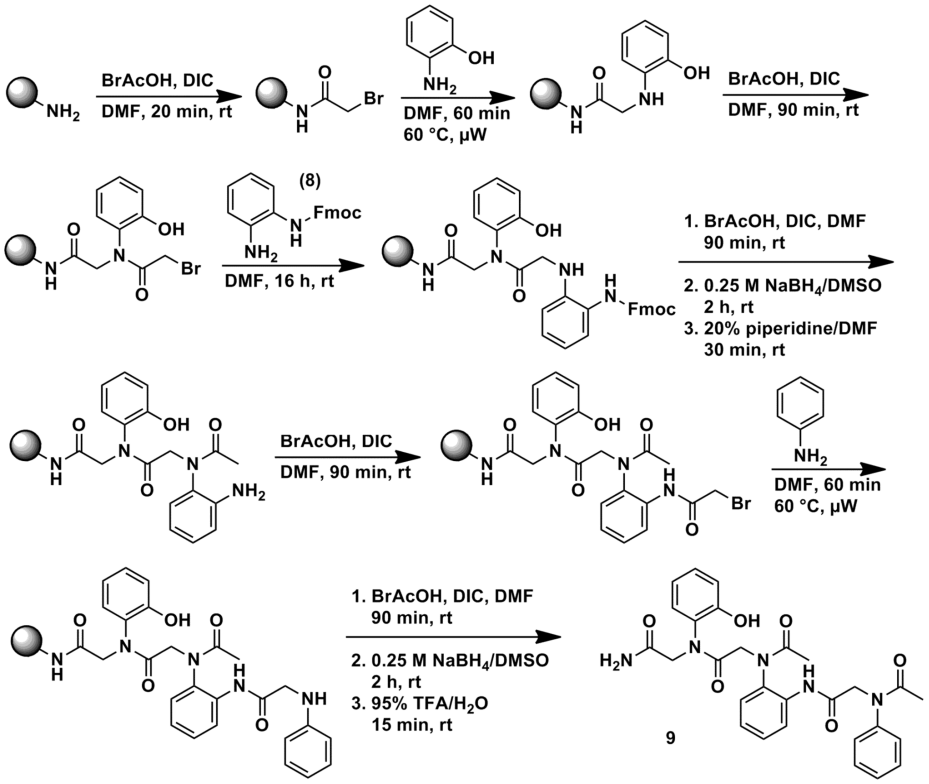

[a]Reagents and conditions: Fmoc-OSu = 9-fluorenylmethyl *N*-succinimidyl carbonate; DMF = *N*,*N*-dimethylformamide; BrAcOH = bromoacetic acid; DIC = *N*,*N*-diisopropylcarbodiimide; DMSO = dimethyl sulfoxide; TFA = trifluoroacetic acid; μW = microwave irradiation; rt = room temperature.

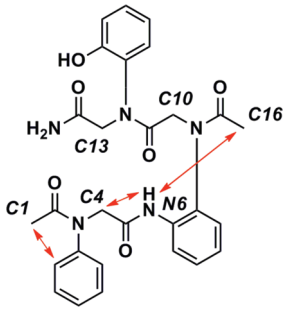

FIGURE 6. Chemical structure of peptoid **9**. Observed NOEs of the major conformer family are indicated by red arrows.

conformer families in $CDCl_3$ at room temperature. 2D rotating-frame Overhauser effect spectroscopy (ROESY) was next utilized to detect NOEs between backbone and side-chain protons on **9** to obtain information about its solution-phase structure. Figure 6 shows important NOEs for the major conformer family of peptoid **9** that indicate the presence of *trans*-amide bonds throughout the peptoid backbone. In *N*-aryl peptoids, a backbone *trans*-amide conformation is characterized by an interresidue NOE from the backbone methylene protons of one residue (*i*) to the *ortho*-aromatic protons of an adjacent residue ($i+1$), while a backbone *cis*-amide conformation is characterized by an interresidue NOE between the backbone methylene protons of one residue (*i*) to the backbone methylene protons of an adjacent residue (*i*-1).[18] In peptoid **9**, there is an NOE from the C1 methyl protons to the *ortho*-aromatic protons in residue 1 and an interresidue NOE from the C4 methylene and the C16 methyl protons to the N6 amide proton. We were not able to unambiguously assign an NOE from the C10 methylene protons to the *ortho*-aromatic proton in residue 3 due to peak overlap in this region of the spectrum. However, we did not observe an interresidue NOE from the C10 methylene protons to the C13 methylene protons, which suggests that residue 3 does not adopt a *cis*-amide conformation. We also note the significant downfield chemical shift of the N6 amide proton at 10.67 ppm, which implies that this proton is involved in a hydrogen bond, presumably to the C11 carbonyl oxygen (vide supra). The presence of such a hydrogen bond would most likely orient the peptoid backbone termini in an approximate antiparallel fashion, as illustrated by the chemical structure in Figure 6 and similar to the solid-state structure of peptoid monomer **2** (Figure 4A). In view of this possible structure, we also anticipated observing a weak NOE between the C13 and C4 hydrogens in peptoid **9**; such a NOE was not apparent, however, even when the ROESY experiment was performed with an extended number of transients and at lower temperature (0 °C; see below).

Characterization of Peptoid 9 in the Solid State. The structure of peptoid turn **9** was further characterized using single-crystal X-ray crystallography. Crystals of **9** were grown by slow evaporation from a mixture of acetone/*n*-hexane. We were pleased to observe that peptoid **9** resembles a reverse-turn structure in the solid state (see Figure 7). This turn can be classified as a δ or C8 turn in the context of

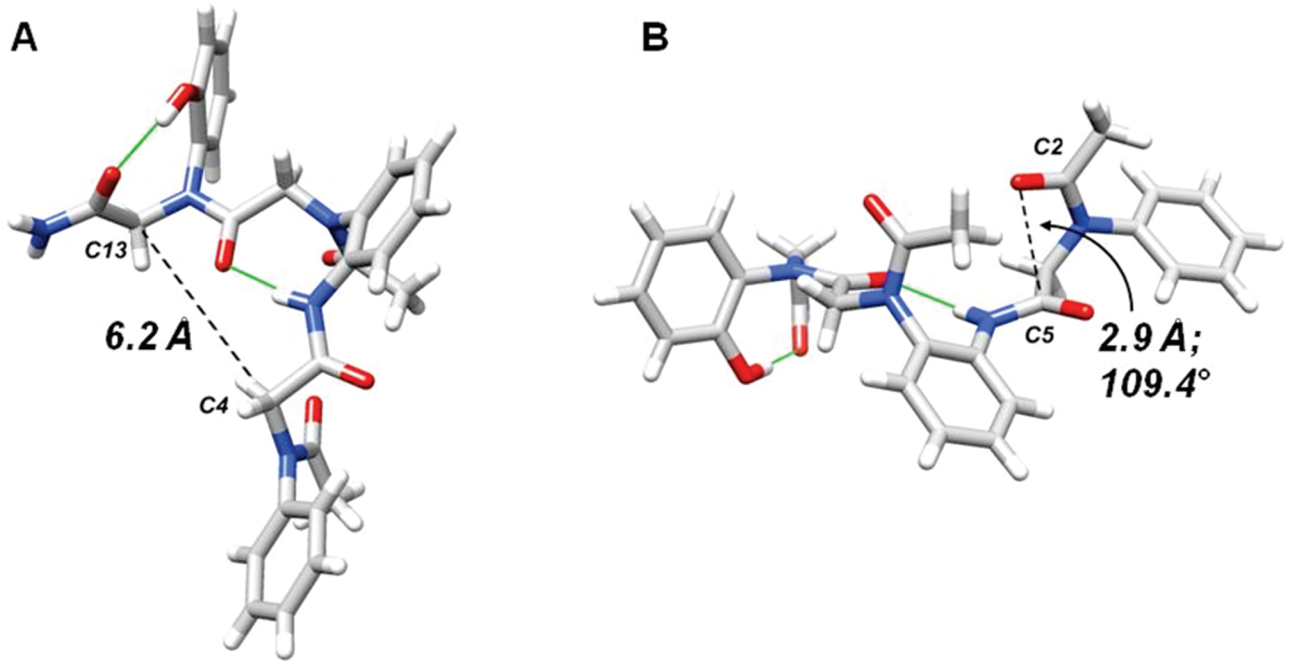

FIGURE 7. X-ray crystal structure of peptoid **9**. (A) Side view of **9** showing C4···C13 distance. (B) End view of **9** showing n→$\pi^*_{C=O}$ backbone interaction. Hydrogen bonds (solid green lines) and interatomic distances (black dashed lines) are shown.

α-peptides, which is defined by an 8-atom hydrogen-bond ring between the amide proton and the carbonyl oxygen of two adjacent residues ($i \rightarrow i \pm 1$ interaction).[52,53] The distance between the ends of the 10-atom turn spanning the C4 methylene carbon to the C13 methylene carbon of peptoid **9** is 6.2 Å, within the 7 Å maximum limit of typical peptide turns.[49,50] Based on the solid-state structure of **9**, we note that the interproton distance between the methylene protons on C13 and the methylene protons on C4 is ~4.5 Å, which is near the approximate threshold distance for NOE observations and may be a contributing factor in our inability to observe a NOE between these two pairs of methylene protons in $CDCl_3$ (as mentioned above). Two intramolecular 8-membered-ring hydrogen bonds are present: one between the side chain hydroxyl proton and C14 carbonyl oxygen and the other between the N6 amide proton and C11 carbonyl oxygen. Notably, both hydrogen bonds in the crystal structure of **9** are also present in the crystal structures of their respective monomers (**2** and **3**), suggesting that these *N*-aryl side chains can also form predictable, intraresidue hydrogen bonds to the peptoid backbone *when incorporated into peptoid oligomers*. These X-ray crystallographic data are significant, as **9** represents the first acyclic peptoid turn, to our knowledge, to be characterized in the solid state.

Further analysis of the solid-state structure of **9** revealed an n→$\pi^*_{C=O}$ stereoelectronic interaction occurring within the peptoid backbone, from the C2 *N*-terminal carbonyl oxygen to the C5 anilide carbonyl (O···C=O distance and angle of 2.9 Å and 109°, respectively; Figure 7B). The n→$\pi^*_{C=O}$ interaction is defined by donation of electron density from a carbonyl oxygen lone pair into the π^* orbital of an adjacent amide carbonyl and has been shown to stabilize the *trans*-amides of tertiary amides.[54−56] Previously, we had characterized a related n→$\pi^*_{C=O}$ interaction in the solid-state structure of a peptoid monomer system. This interaction occurred between a carbonyl oxygen in the peptoid backbone and an adjacent *p*-NO_2 anilide carbonyl in the side chain.[30] To our knowledge, the n→$\pi^*_{C=O}$ interaction in **9** represents the first solid-state example of an n→$\pi^*_{C=O}$ interaction *occurring exclusively within a peptoid backbone*. Note, this n→$\pi^*_{C=O}$ interaction is absent in the solid-state structure of monomer **1**, presumably due to the poorer electron accepting ability of the carbonyl π^* orbital of the tertiary piperidinyl amide in **1** relative to the carbonyl π^* orbital of the secondary aryl amide in oligomer **9**.[34] While the n→π^* interaction is not as energetically significant as other noncovalent interactions (typically < 1 kcal/mol in a peptoid monomer),[30,34] the crystal structure of **9** illustrates that the n→$\pi^*_{C=O}$ interaction can exist in polypeptoids containing *trans*-amides and should be considered among the repertoire of noncovalent interactions that influence overall peptoid structure.

Lastly, we note that peptoid **9** is an approximate modular assembly of the peptoid residues studied in model systems **1**−**3**, even in view of the nonstandard backbone linkage of residues 1 and 2 via the side chain. Thus, we compared the

TABLE 2. Dihedral Angles Observed in X-ray Crystal Structure of Peptoid 9

residue	ϕ (deg)	ψ (deg)	χ_1 (deg)	ω (deg)
1	−67.75	140.09	116.26	177.58
2	73.71	−158.88	103.96	176.70
3	82.97	178.44	103.73	−176.05

(52) Chou, K.-C. *Anal. Biochem.* **2000**, *286*, 1–16.
(53) Stroup, A. N.; Rockwell, A. L.; Rheingold, A. L.; Gierasch, L. M. *J. Am. Chem. Soc.* **1988**, *110*, 5157–5161.
(54) Choudhary, A.; Gandla, D.; Krow, G. R.; Raines, R. T. *J. Am. Chem. Soc.* **2009**, *131*, 7244–7246.
(55) Hodges, J. A.; Raines, R. T. *Org. Lett.* **2006**, *8*, 4695–4697.
(56) Horng, J.-C.; Raines, R. T. *Protein Sci.* **2006**, *15*, 74–83.

backbone dihedral angles in the solid-state structures of monomers **1**−**3** versus those in trimer **9** to acquire insights into the local torsional preferences of each *N*-aryl side chain in monomeric versus oligomeric peptoids (Tables 1 and 2). Analysis of the dihedral angles in peptoid oligomer **9** reveals that the ψ and ϕ angles for the *N*-terminal residue 1, which contains an unsubstituted *N*-aryl side chain, deviate the most relative to the corresponding peptoid monomer (**1**). Specifically, there is a 33.25° difference in the ϕ angle and a 27.70° difference in the ψ angle between **1** and the corresponding residue in peptoid oligomer **9**. Residues 2 and 3, both comprising *ortho*-substituted hydrogen-bonding *N*-aryl side chains, show a less significant change in their respective ψ and ϕ dihedral angles compared to the corresponding monomers. In residue 2 of **9**, there is a 5.50° difference in the ϕ angle and a 3.57° difference in the ψ angle compared to model peptoid **3**. In residue 3 of peptoid **9**, there is a 8.42° difference in the ϕ angle and a 13.17° difference in the ψ angle compared to model peptoid **3**. Overall, these comparisons of torsional angles in peptoids **1**−**3** and **9** suggest that there is more rotational flexibility in the ψ and ϕ dihedral angles of residues containing an unsubstituted *N*-aryl side chain relative to residues with *ortho*-substituted hydrogen-bonding *N*-aryl side chains. These data support the work of Butterfoss et al.,[32] whose previous survey of (experimentally determined) *N*-alkyl and *N*-aryl peptoid structures illustrated the flexibility of the ψ angle in peptoids when the backbone amide bond is in the *trans* conformation. The greater variations in the dihedral angles of residue 1, relative to residues 2 and 3 in peptoid **9**, may be a result of the backbone orientation required for residue 1 to participate in the observed $n\rightarrow\pi^*_{C=O}$ interaction. In peptoid **9**, residue 1 contains an unsubstituted *N*-aryl side chain that cannot participate in intramolecular hydrogen bonding. Presumably, the absence of an *ortho*-positioned hydrogen bond permits more rotational freedom in the backbone of residue 1, relative to the hydrogen-bond containing residues 2 and 3, thus allowing residue 1 to assume a proper orientation for an $n\rightarrow\pi^*_{C=O}$ interaction.

Summary and Outlook. We have outlined a new design strategy for the construction of discretely folded peptoids that utilizes *N*-aryl side chains with *ortho*-substituents capable of hydrogen-bond donation. These *N*-aryl side chains enforce *trans*-amide geometries within the peptoid backbone and participate in localized hydrogen bonds to their respective intraresidue backbone carbonyl oxygens. Conformational analyses of a series of peptoid monomers in solution and in the solid state revealed that hydrogen-bonding *N*-aryl side chains can be used to effectively modulate local dihedral angles in peptoids. We examined these side chains in the context of a peptoid trimer and demonstrated that they can be used to effectively introduce a reverse-turn conformation. Together, our results reveal a new tactic for the design of well-folded peptoids that should be applicable to the assembly of peptoids with distinct secondary structures. Specifically, we envisage peptoids that contain multiple *N*-aryl side chains with *ortho*-hydrogen-bond donors could adopt highly stable, polyproline-type II peptoid helices. Even more interesting may be the incorporation of adjacent α-chiral and *N*-aryl side chains into peptoids, which could potentially enforce a particular *N*-aryl atropisomer, and thereby further reduce overall conformational heterogeneity. Ongoing work in our laboratory is focused on optimizing and applying these design strategies to generate novel peptoid architectures and expand the known, three-dimensional peptoid structure space.

Experimental Section

General Methods. All reagents and solvents were purchased from commercial sources and used without further purification, with the exception of dichloromethane (CH_2Cl_2) and hexanes, which were distilled immediately prior to use. Thin-layer chromatography (TLC) was performed on silica gel 60 F254 plates. Silica gel 60 (40−63 μm) was used for flash column chromatography.[57]

^{1}H NMR (500 MHz) and ^{13}C NMR (125 MHz) spectra were recorded on 500 MHz spectrometers in deuterated solvents. ^{1}H NMR (300 MHz) and ^{13}C NMR (75 MHz) spectra were recorded on 300 MHz spectrometers in deuterated solvents. Rotating-frame Overhauser effect spectroscopy (ROESY) NMR experiments were performed on a 600 MHz spectrometer using a 5 mm hcn probe and were referenced to solvent. Chemical shifts are reported in parts per million (ppm, δ) using tetramethylsilane (TMS) as a reference (0.0 ppm). Couplings are reported in hertz. All NMR data were manipulated and processed using standard NMR software.[58]

Attenuated total reflectance (ATR)-IR spectra were recorded with an IR spectrometer outfitted with a single-reflection ATR unit and a ZnSe crystal with a spectral range of 20000 to 650 cm^{-1}. Electrospray ionization (ESI) mass spectra were obtained on a mass spectrometer equipped with a time-of-flight analyzer. Samples were dissolved in methanol and sprayed with a sample cone voltage of 20. Perfluorokerosene (PFK) was used for calibration. Matrix-assisted laser desorption/ionization time-of-flight (MALDI-TOF) mass spectra were obtained on a mass spectrometer equipped with a 337 nm laser and a reflectron. In positive-ion mode, the acceleration voltage was 25 kV.

Analytical HPLC analyses were performed using a laboratory HPLC system equipped with a UV/vis detector. Purities were determined by integration of peaks at 220 nm. A C18 column (4.6 mm × 250 mm) was used for all analytical HPLC work. Standard HPLC conditions were as follows: flow rate = 1 mL/min; mobile phase A = 0.1% trifluoroacetic acid (TFA) in water; mobile phase B = 0.1% TFA in acetonitrile. LC−MS data were obtained using a laboratory HPLC system equipped with an UV/vis diode array detector and a single quadrupole analyzer (ESI). A C18 wide-pore column (15 cm × 2.1 mm) was used for all LC−MS work. Standard HPLC conditions for LC−MS were as follows: flow rate = 200 μL/min; mobile phase A = 0.1% formic acid in water; mobile phase B = 0.1% formic acid in acetonitrile.

Representative Synthetic Route to Model Peptoids 1−7. 2-Bromo-1-(piperidin-1-yl)ethanone (200 mg, 0.97 mmol; prepared according to our previously reported method)[30] was dissolved in dry DMF (2 mL) in a dry 50 mL flask equipped with a dropping funnel. Aniline (88 μL, 0.97 mmol) was dissolved in dry DMF (5 mL) and added dropwise via the dropping funnel to the stirred solution. The reaction mixture was allowed to stir for 6 h at room temperature. The DMF was removed *in vacuo*, and the resulting crude oil was redissolved in CH_2Cl_2 (10 mL) and cooled to 0 °C under stirring. Triethylamine (406 μL, 2.91 mmol) was added to the stirred solution, followed by the dropwise addition of an acetyl chloride/CH_2Cl_2 solution (429 μL, 1.96 mmol in ∼5 mL of CH_2Cl_2). The reaction mixture was allowed to return to room temperature and stirred for an additional 15 min. Thereafter, the reaction mixture was transferred

(57) Still, W. C.; Kahn, M.; Mitra, A. *J. Org. Chem.* **1978**, *43*, 2923–2925.
(58) Goddard, T. D.; Kneller, D. G. SPARKY, v. 3.110; University of California, San Francisco.

to a separatory funnel, washed with 10% w/v aq citric acid (1×), satd aq $NaHCO_3$ (1×), and dried over anhydrous $MgSO_4$. The solvent was removed in vacuo, and the crude peptoid product was purified to homogeneity by flash silica gel chromatography (EtOAc).[57] To generate model peptoids **2** and **4**, the aryl hydroxyl groups (protected as methoxyl groups) were deprotected using BBr_3 in a final step according to a literature procedure.[59] Isolated yields: **1**, 70%; **2**, 45%; **3**, 37%; **4**, 51%; **5**, 40%, **6**, 78%; **7**, 73%.

Peptoid 1. TLC: R_f = 0.33 (EtOAc). ^{1}H NMR (500 MHz, $CDCl_3$): δ 7.44−7.38 (m, 4H), 7.33 (tt, J = 7.0, 1.7 Hz, 1H), 4.48 (s, 3H), 3.56 (m, 2H), 3.37 (m, 2H), 1.95 (s, 3H), 1.69−1.54 (m, 6H). ^{13}C NMR (75 MHz, $CDCl_3$, ^{1}H broadband-decoupled): δ 171.0, 166.0, 144.0, 129.7, 128.4, 128.1, 51.3, 46.0, 43.4, 26.4, 25.6, 24.6, 22.5. IR (ATR, cm^{-1}): 3006, 2938, 2864, 2821, 1646, 1596, 1494, 1477, 1461, 1443, 1418, 1390, 1359, 1346, 1265, 1253, 1237, 1225, 1156, 1142, 1227, 1108, 1056, 1033, 1011, 902, 855, 844, 834, 803, 772, 729, 701, 647, 617. HRMS (ESI): calcd for $C_{15}H_{20}N_2O_2Na$ m/z 283.1417, found m/z 283.1420.

Peptoid 2. TLC: R_f = 0.29 (EtOAc). ^{1}H NMR (500 MHz, $CDCl_3$): δ 11.20 (s, 1H), 8.43 (d, J = 8.3 Hz, 1H), 7.36 (m, 1H), 7.10 (m, 2H), 5.18 (d, J = 16.0 Hz, 1H), 3.60 (m, 2H), 3.55 (d, J = 16.0 Hz, 1H), 3.45 (ddd, J = 13.6, 7.5, 3.5 Hz, 2H), 3.36 (ddd, J = 13.6, 7.5, 3.5 Hz, 2H), 2.25 (s, 3H), 1.84 (s, 3H), 1.76−1.50 (m, 6H). ^{13}C NMR (75 MHz, $CDCl_3$, ^{1}H broadband-decoupled): δ 171.8, 170.1, 167.5, 137.4, 132.8, 129.8, 128.1, 124.3, 122.5, 51.6, 46.2, 43.8, 26.3, 25.6, 24.7, 24.5, 21.5. IR (ATR, cm^{-1}): 2936, 1700, 1659, 1634, 1541, 1456, 1387, 1311, 1257, 1022, 799, 768, 749, 688. HRMS (ESI): calcd for $C_{17}H_{23}N_3O_3Na$ m/z 340.1632, found m/z 340.1628.

Peptoid 3. TLC: R_f = 0.4 (3:1 EtOAc/hexane). ^{1}H NMR (500 MHz, $CDCl_3$): δ 10.85 (s, 1H), 7.28 (td, J = 7.8, 1.6 Hz, 1H), 7.05 (dd, J = 4.4, 1.6 Hz, 1H), 7.03 (dd, J = 4.4, 1.6 Hz, 1H), 6.87 (td, J = 7.8, 1.4 Hz, 1H), 5.25 (d, J = 16.1 Hz, 1H), 3.65−3.55 (m, 2H), 3.55 (d, J = 16.1 Hz, 1H), 3.45 (ddd, J = 13.4, 7.7, 3.5 Hz, 2H), 3.37 (ddd, J = 13.4, 7.7, 3.5 Hz, 2H), 1.90 (s, 3H), 1.77−1.50 (m, 6H). ^{13}C NMR (75 MHz, $CDCl_3$, ^{1}H broadband-decoupled): δ 172.3, 168.6, 155.1, 130.8, 130.6, 128.7, 120.5, 119.0, 51.2, 46.3, 44.1, 26.3, 25.5, 24.4, 21.5. IR (ATR, cm^{-1}): 2951, 2856, 1663, 1624, 1494, 1453, 1406, 1314, 1293, 1256, 1140, 1021, 988, 835, 799, 761, 751, 628. HRMS (ESI): calcd for $C_{15}H_{20}N_2O_3Na$ m/z 299.1367, found m/z 299.1364.

Peptoid 4. TLC: R_f = 0.3 (12% MeOH/EtOAc). ^{1}H NMR (300 MHz): δ 8.49 (s 1H), 7.56 (AA′XX′ peak, J_{ax} = 8.6, $J_{aa'}$ = $J_{xx'}$ = 2.4, $J_{ax'}$ = 0.2 Hz, 2H), 7.32 (AA′XX′ peak, J_{ax} = 8.6, $J_{aa'}$ = $J_{xx'}$ = 2.4, $J_{ax'}$ = 0.2 Hz, 2H), 4.46 (s, 2H), 3.52 (m, 2H), 3.36 (m, 2H), 2.17 (s, 3H), 1.92 (s, 3H), 1.72−1.45 (m, 6H). ^{13}C NMR (75 MHz, $CDCl_3$, ^{1}H broadband-decoupled): δ 171.2, 168.8, 166.1, 139.6, 138.0, 129.0, 120.9, 51.3, 46.1, 43.4, 26.4, 25.6, 24.7, 24.6, 22.5. IR (ATR, cm^{-1}): 3435, 3302, 3265, 3194, 3123, 3069, 3008, 2942, 2855, 1692, 1662, 1636, 1606, 1539, 1513, 1455, 1409, 1390, 1371, 1312, 1254, 1233, 1140, 1126, 1112, 1035, 1015, 989, 954, 905, 853, 797, 765, 666, 578, 555. HRMS (ESI): calcd for $C_{17}H_{23}N_3O_3Na$ m/z 340.1632, found m/z 340.1639.

Peptoid 5. TLC: R_f = 0.2 (19:1 EtOAc/MeOH). ^{1}H NMR (300 MHz, $CDCl_3$): δ 7.53 (brs, 1H), 7.15 (AA′XX′ peak, J_{ax} = 8.8, $J_{aa'}$ = $J_{xx'}$ = 2.5, $J_{ax'}$ = 0.2 Hz, 2H), 6.72 (AA′XX′ peak, J_{ax} = 8.8, $J_{aa'}$ = $J_{xx'}$ = 2.5, $J_{ax'}$ = 0.2 Hz, 2H), 4.49 (s, 2H), 3.82 (s, 3H), 3.54 (m, 2H), 3.42 (m, 2H), 1.91 (s, 3H), 1.71−1.49 (m, 6H). ^{13}C NMR (75 MHz, $CDCl_3$, ^{1}H broadband-decoupled): δ 174.0, 168.1, 158.8, 136.6, 130.3, 117.2, 52.6, 47.1, 44.5, 27.4, 26.8, 25.5, 22.3. IR (ATR, cm^{-1}): 3271, 3028, 3010, 2945, 2861, 1643 (broad), 1594, 1514, 1447, 1393, 1317, 1274, 1264, 1254, 1229, 1219, 1214, 1165, 1140, 1127, 1114, 1098, 1034, 1015, 990, 954, 906, 844, 826, 795, 777, 771, 760, 743, 707, 667, 649. HRMS (ESI): calcd for $C_{15}H_{20}N_2O_3Na$ m/z 299.1367, found m/z 299.1359.

Peptoid 6. TLC: R_f = 0.25 (EtOAc). ^{1}H NMR (300 MHz, $CDCl_3$): δ 7.67−7.64 (m, 1H), 7.29−7.20 (m, 3H), 5.08 (d, J = 15.7 Hz, 1H), 3.62 (d, J = 15.7 Hz, 1H), 3.57−3.28 (m, 4H), 2.27 (s, 3H), 1.84 (s, 3H), 1.69−1.45 (m, 6H). ^{13}C NMR (75 MHz, $CDCl_3$, ^{1}H broadband-decoupled): δ 171.3, 165.9, 142.6, 135.5, 131.3, 130.0, 128.6, 127.6, 50.1, 46.1, 43.4, 26.4, 25.6, 24.6, 22.1, 17.8. IR (ATR, cm^{-1}): 3004, 2999, 2934, 2855, 1653, 1601, 1581, 1492, 1456, 1414, 1386, 1358, 1276, 1260, 1227, 1198, 1158, 1139, 1125, 1037, 1024, 1015, 985, 954, 923, 853, 805, 765, 750, 733, 632, 627. HRMS (ESI): calcd for $C_{16}H_{22}N_2O_2Na$ m/z 297.1574, found m/z 297.1567.

Peptoid 7. TLC: R_f = 0.15 (EtOAc). ^{1}H NMR (300 MHz, $CDCl_3$): δ 7.30−7.12 (m, 4H), 4.44 (s, 2H), 3.54 (m, 2H), 3.36 (m, 2H), 2.37 (s, 3H), 1.93 (s, 3H), 1.68−1.51 (m, 6H). ^{13}C NMR (75 MHz, $CDCl_3$, ^{1}H broadband-decoupled): δ 171.1, 166.1, 144.1, 139.8, 129.5, 128.9 (broad), 125.4, 51.3, 46.1, 43.4, 26.4, 25.6, 24.7, 22.5, 21.5. IR (ATR, cm^{-1}): 2932, 2853, 1654, 1604, 1588, 1489, 1443, 1314, 1253, 1227, 1186, 1138, 1111, 1090, 1038, 1015, 988, 954, 925, 892, 853, 787, 760, 720, 702. HRMS (ESI): calcd for $C_{16}H_{22}N_2O_2Na$ m/z 297.1574, found m/z 297.1567.

Synthesis of Amine 8 (9*H*-Fluoren-9-yl)methyl 2-Aminophenylcarbamate). 1,2-Phenylenediamine (200 mg, 1.85 mmol) was dissolved in dry DMF (10 mL) in a dry 50 mL flask equipped with a dropping funnel. 9-Fluorenylmethyl *N*-succinimidyl carbonate (Fmoc-OSu, 624 mg, 1.85 mmol) was dissolved in dry DMF (10 mL) and added dropwise via the dropping funnel to the stirred solution. The reaction mixture was allowed to stir for 2 h at room temperature. The solvent was removed in vacuo, and the crude product was purified to homogeneity by flash silica gel chromatography (2:1 hexanes/EtOAc) to give 200 mg of **8** as a white solid. Isolated yield: 33%.

Amine 8. TLC: R_f = 0.3 (2:1 hexane/EtOAc). ^{1}H NMR (300 MHz, DMSO-d_6): δ 8.70 (brs, 1H), 7.90 (d, J = 7.3 Hz, 2H), 7.74 (m, 2H), 7.43 (t, J = 7.3 Hz, 2H), 7.34 (t, J = 7.3 Hz, 2H), 7.12 (m, 1H), 6.89 (td, J = 7.5,1.4 Hz, 1H), 6.71 (dd, J = 7.9,1.4 Hz, 1H), 6.53 (td, J = 7.5,1.4 Hz, 1H), 4.87 (s, 2H), 4.40 (d, J = 6.9 Hz, 2H), 4.29 (t, J = 6.9 Hz, 1H). ^{13}C NMR (75 MHz, DMSO-d_6, ^{1}H broadband-decoupled): δ 155.1, 144.5, 142.6, 141.5, 128.3, 127.8, 126.3, 126.0 (broad), 123.7, 120.8, 116.9, 116.3, 66.4, 47.4. IR (ATR, cm^{-1}): 3428, 3352, 1680, 1648, 1623, 1597, 1530, 1498, 1465, 1454, 1311, 1291, 1272, 1254, 1233, 1161, 1106, 1094, 1051, 1041, 987, 938, 860, 799, 755, 751, 682. MS (ESI): calcd m/z 330.1, found m/z 330.9 $[M + H]^+$.

Synthesis and Characterization of Peptoid 9. Peptoid **9** was synthesized using a modified version of a previously reported, microwave-assisted solid-phase method on Rink-amide derivatized polystyrene resin.[51] The crude peptoid was purified by flash silica gel chromatography (eluent: 10% MeOH/EtOAc, R_f = 0.31) and characterized by MS to confirm its identity. MALDI-TOF MS: calcd m/z 531.2, found m/z 554.1 $[M + Na]^+$. See the Supporting Information for HPLC, MS, and NMR data for peptoid **9**.

NMR Analysis for Peptoid Monomers 1−7. 1D-NOESY spectra were used to identify *cis*/*trans* amide rotameric peaks, as reported in our previous studies.[30,34] The *cis*/*trans* amide ratios were determined by integration of 1D ^{1}H NMR spectra.

NMR Analyses for Peptoid 9. Peptoid **9** was dissolved in $CDCl_3$ to give a ∼10−20 mM solution. 2D-ROESY experiments on **9** was performed at 25 °C using the following parameter values: mix time = 200 ms; spectral width = 8000 Hz; number of transients (nt) = 16; number of increments (ni) = 400. The number of points (np) was 2048, and 192 points were obtained by linear prediction in the f1 dimension. Square cosine window functions were applied in both dimensions. The spectra were zero-filled to generate f1f2 matrices of 4096 × 4096 points.

(59) Vickery, E. H.; Pahler, L. F.; Eisenbraun, E. J. *J. Org. Chem.* **1979**, *44*, 4444–4446.

NOE intensities for **9** were classified according to their relative cross-peak integrations in the 2D-ROESY spectrum.

X-ray Crystal Structure Data for 1−3 and 9. Model peptoids **1**−**3** and oligomer **9** (∼10 mg) were each dissolved in *n*-hexane with a minimal amount of either CH_2Cl_2 (**1**−**3**) or HPLC-grade acetone (**9**). Slow evaporation afforded crystals suitable for X-ray analysis after ∼2−3 days. For all four X-ray structures, non-hydrogen atoms were refined with anisotropic displacement coefficients. All hydrogen atoms were included in the structure factor calculations at idealized positions and were allowed to ride on the neighboring atoms with relative isotropic displacement coefficients. All software and sources of the scattering factors are contained in the program suite SHELXL.[60]

X-ray crystal data for 1: $C_{15}H_{20}N_2O_2$, monoclinic, $P2_1$, a = 8.116(3) Å, b = 8.813(3) Å, c = 10.402(3) Å, β = 112.059(4)°, V = 689.6(4) Å^3, Z = 2, T = 100(2) K, D_{calc} = 1.254 mg/m^3, R(F) based on F^2 for $I \geq 2\sigma$ = 4.27% for 3873 independent reflections (2.11° ≤ θ ≤ 30.02°).

X-ray crystal data for 2: $C_{15}H_{20}N_2O_3$, monoclinic, $P2_1/c$, a = 8.6600(2) Å, b = 29.0866(7) Å, c = 11.5414(3) Å, β = 91.7060(10)°, V = 2905.87(12) Å^3, Z = 8, T = 103(2) K, D_{calc} = 1.263 mg/m^3, R(F) based on F^2 for $I \geq 2\sigma$ = 3.49% for 5465 independent reflections (3.04° ≤ θ ≤ 69.92°).

X-ray crystal data for 3: $C_{17}H_{23}N_3O_3$, triclinic, $P\bar{1}$, a = 8.7424(3) Å, b = 12.4268(4) Å, c = 15.4933(5) Å, α = 81.016(2)°, β = 81.487(2)°, γ = 84.078(2)°, V = 1638.70(9) Å^3, Z = 4, T = 103(2) K, D_{calc} = 1.286 mg/m^3, R(F) based on F^2 for $I \geq 2\sigma$ = 3.69% for 5875 independent reflections (2.91° ≤ θ ≤ 69.76°). The hydrogen atoms H(3N) and H(6N) attached to nitrogen atoms were located in the difference map and were refined independently.

X-ray crystal data for (9): $C_{31}H_{35}N_5O_7$, triclinic, $P\bar{1}$, a = 10.7078(10) Å, b = 12.1574(13) Å, c = 13.2918(12) Å, α = 107.653(7)°, β = 109.664(7)°, γ = 93.441(8)°, V = 1527.1(3) Å^3, Z = 2, T = 100(2) K, D_{calc} = 1.282 mg/m^3, R(F) based on F^2 for $I \geq 2\sigma$ = 9.26% for 5293 independent reflections (3.88° ≤ θ ≤ 69.05°).

Acknowledgment. We thank the NSF (CHE-0449959), ONR (N000140710255), Greater Milwaukee Foundation, Burroughs Welcome Fund, and Research Corporation for financial support of aspects of this work. H.E.B. is an Alfred P. Sloan Foundation fellow. Support for the NMR facilities at UW—Madison by the NIH (1 S10 RR13866-01 and 1 S10 RR08389-01) and the NSF (CHE-0342998 and CHE-9629688) is gratefully acknowledged. X-ray crystal structures were visualized using the UCSF Chimera package from the Resource for Biocomputing, Visualization, and Informatics at the University of California, San Francisco (supported by NIH P41 RR-01081). We thank Dr. Charlie Fry and Dr. Monika Ivancic for assistance with NMR spectroscopy, Lara Spencer for X-ray crystallographic work, and Prof. Hans Reich, Prof. Samuel Gellman, and Dr. Benjamin Gorske for many contributive discussions.

Supporting Information Available: NMR data for compounds **1**−**9**, HPLC data for peptoid **9**, and X-ray crystallographic data (CIF). This material is available free of charge via the Internet at http://pubs.acs.org.

(60) Sheldrick, G. M. *Acta Crystallogr.* **2008**, *A64*, 112–122.